New eco-friendly corrosion inhibitors based on azo rhodanine derivatives for protection copper corrosion

A.M. Eldesoky[1], M.A. El-Bindary[1], A.Z. El-Sonbati[2,*], Sh.M. Morgan[3]

[1] *Engineering Chemistry Department, High Institute of Engineering & Technology, Damietta, Egypt*

[2] *Chemistry Department, Faculty of Science, Damietta University, Damietta 34517, Egypt*

[3] *Environmental Monitoring Laboratory, Ministry of Health, Port Said, Egypt*

[*] *Corresponding author: E-mail: elsonbatisch@yahoo.com (A.Z. El-Sonbati). Tel.: +2 01060081581; Fax: +2 0572403868*

Abstract

The inhibitive action of some new azo rhodanine derivatives, namely 5-(4'-methoxyphenylazo)-2-thioxo-4-thiazolidinone (I), 5-(phenylazo)-2-thioxo-4-thiazolidinone (II) and 5-(4'-nitrophenylazo) -2-thioxo-4-thiazolidinone (III) against the corrosion of copper in 2 M HNO_3 solution has been investigated using weight loss, Tafel polarisation, electrochemical impedance spectroscopy (EIS) and electrochemical frequency modulation (EFM) techniques. The inhibition efficiency increased with increasing inhibitor concentrations and decreased with increasing temperature. Potentiodynamic polarisation studies clearly showed that these compounds acted as mixed inhibitors. The ability of the molecule to adsorb on the copper surface obeyed Freundlich adsorption isotherm and was dependent on the active centres and molecular size of the molecules. The thermodynamic activation parameters of the copper corrosion in 2 M HNO_3 were determined and discussed. Molecular modelling was used to gain some insight, about structural and electronic effects in relation to the inhibiting efficiencies. Inhibition efficiency values obtained from various methods employed were in reasonable agreement.

1. Introduction

Copper is widely used in many applications in microelectronic industries and communication as a conductor in electrical power lines, pipelines for domestic and industrial water utilities including sea water, heat conductors, and fabrication of heat exchangers due to its excellent electrical and thermal conductivities, low cost and its good mechanical workability [1,2]. Therefore, considerable attention has been drawn during the past few decades to inhibit corrosion of copper. Corrosion inhibition of copper can be achieved through the modification of its interface by forming self assembled ordered ultrathin layers of organic inhibitors. Efficient inhibitors for copper are heterocyclic organic compounds consisting of a π-system and P, S, N, or O heteroatom. It is noticed that presence of these functional groups and heteroatom in the organic compound molecules improves its action as copper corrosion inhibitor because they enable chemisorptions, such as azoles [3-7], amines [8], amino acids [9] and organic derivatives also offer special affinity to inhibit corrosion of various metals in different acidic media [10,11]. Copper is relatively noble metal, requiring strong oxidants for its corrosion or dissolution. Nitric acid is a strong copper oxidizer capable of rapidly attacking copper, so various corrosion inhibitors were suggested for copper inhibition in nitric acid solutions. However, it remains an important objectives that one can either find a new inhibitor or to improve the efficiency of a known inhibitor by applying a synergistic technique.

In this paper the EFM is used as a new non-linear distortion technique, evaluated as an instantaneous corrosion monitoring technique and is used here for online monitoring of corrosion rate of copper in the absence and presence of investigated compounds. The purpose of this paper is to compare the corrosion inhibition data derived from EFM with that obtained from Tafel extrapolation, EIS and weight loss techniques.

2. Materials and methods

2.1. Composition of material samples

The chemical composition of the copper in weight % listed in Table 1.

Table 1: Chemical composition of the copper (weight %)

Element	Sn	Ag	Fe	Bi	Pb	As	Cu
Weight %	0.001	0.001	0.01	0.0005	0.002	0.0002	The rest

2.2. Chemicals and solutions
Nitric acid (BDH grade) and organic additives. The organic inhibitors used in this study were some 4-thiazolidinone derivatives are listed in Table 2.

In a typical preparation, 25 ml of distilled water containing 0.01 mol hydrochloric acid was added to aniline (0.01 mol) or *p*-derivatives. To the resulting mixture stirred and cooled to 0 °C, a solution of 0.01 mol sodium nitrite in 20 ml of water was added dropwise. The formed diazonium chloride was consecutively coupled with an alkaline solution of 0.01 mol 2-thioxo-4-thiazolidinone, in 10 ml of pyridine as shown in Scheme 1 [12-16]. The color precipitate was filtered through sintered glass crucible and washed several times with water and ether. The crude products were purified by recrystallization from hot ethanol and dried in a vacuum desiccator over P_2O_5.
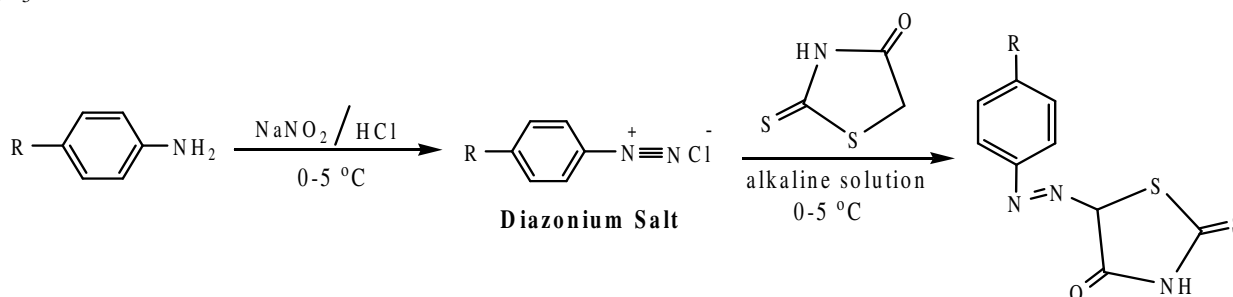
R = -OCH$_3$ (I), -H (II) and -NO$_2$ (III)
Scheme 1. The formation mechanism of azo rhodanine derivatives.

2.3. Methods used for corrosion measurements
2.3.1. Electrochemical Frequency Modulation technique
EFM experiments were performed with applying potential perturbation signal with amplitude 10 mV with two sine waves of 2 and 5 Hz. The choice for the frequencies of 2 and 5 Hz was based on three arguments [17]. The larger peaks were used to calculate the corrosion current density (i_{corr}), the Tafel slopes (β_c and β_a) and the causality factors CF-2 and CF-3 [18].

All electrochemical experiments were carried out using Gamry instrument PCI300/4 Potentiostat/Galvanostat/Zra analyzer, DC105 corrosion software, EIS300 electrochemical impedance spectroscopy software, EFM140 electrochemical frequency modulation software and Echem Analyst 5.5 for results plotting, graphing, data fitting and calculating.
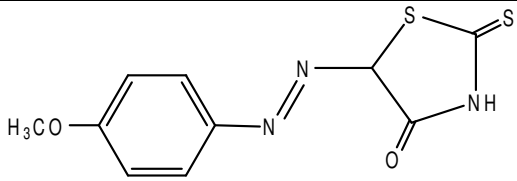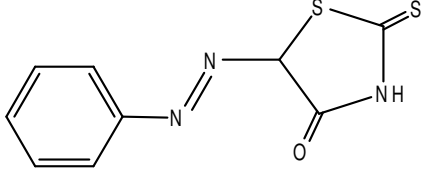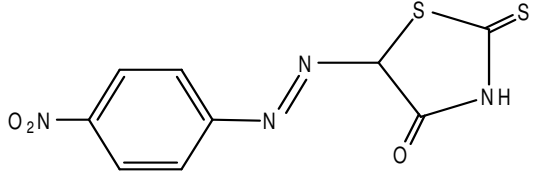
2.3.2. Electrochemical Impedance Spectroscopy measurements
Impedance measurements were carried out using AC signals of 5 mV peak to peak amplitude at the open circuit potential in the frequency range of 100 kHz to 0.1 Hz. All impedance data were fitted to appropriate equivalent circuit using the Gamry Echem Analyst software.

2.3.3. Potentiodynamic polarization measurements
Polarization experiments were carried out in a conventional three-electrode cell with platinum gauze as the auxiliary electrode (1 cm^2) and a saturated calomel electrode (SCE) coupled to a fine Luggin capillary as reference electrode. The working electrode was in the form of a square cut from copper sheet of equal composition embedded in epoxy resin of poly(tetrafluoroethylene) so that the flat surface area was 1 cm^2. Prior to each measurement, the electrode surface was pretreated in the same manner as the weight loss experiments. Before measurements, the electrode was immersed in solution at natural potential for 30 min. until a steady state was reached. The potential was started from – 600 to + 400 mV vs. open circuit potential (E_{ocp}). All experiments were carried out in freshly prepared solutions at 30 °C and results were always repeated at least three times to check the reproducibility.

Table 2: Chemical structures, names, molecular weights and molecular formula of compounds (I-III)

Compound	Structure	Empirical formula	Molecular weight
I	5-(4'-Methoxyphenylazo)-2-thioxo-4-thiazolidinone	$C_{10}H_9N_3O_2S_2$	267
II	5-(Phenylazo)-2-thioxo-4-thiazolidinone	$C_9H_7N_3OS_2$	237
III	5-(4'-Nitrophenylazo)-2-thioxo-4-thiazolidinone	$C_9H_6N_4O_3S_2$	282

2.3.4. Weight loss measurements

For weight loss measurements, square specimens of size 2 cm × 2 cm × 2 cm were used. The specimens were first polished to a mirror finish using 400 and 800 grit emery paper, immersed in methanol and finally washed with bidistilled water and dried before being weighed and immersed into the test solution. The weight loss measurements were carried out in a 100 ml capacity glass beaker placed in water thermostat. The specimens were then immediately immersed in the test solution without or with desired concentration of the investigated compounds. Triplicate specimens were exposed for each condition and the mean weight losses were reported in order to verify reproducibility of the experiments.

2.3.5. Theoretical study

The molecular structures of the investigated compounds were optimized initially with PM3 semiempirical method so as to speed up the calculations. The resulting optimized structures were fully re-optimized using ab initio Hartree–Fock (HF) [19] with 6-31G basis set. The molecules were built with the Gauss View 3.09 and optimized using Gaussian 03W program [20].

3. Results and discussion

3.1. Electrochemical Frequency Modulation Technique (EFM)

EFM is a non-destructive corrosion measurement technique that can directly and quickly determine the corrosion current values without prior knowledge of Tafel slopes, and with only a small polarizing signal. These advantages of EFM technique make it an ideal candidate for online corrosion monitoring [21]. The great strength of the EFM is the causality factors which serve as an internal check on the validity of EFM measurement. The causality factors CF-2 and CF-3 are calculated from the frequency spectrum of the current responses.

Figure 1 shows the EFM intermodulation spectrums of copper in nitric acid solution containing different concentrations of compound (I). Similar curves were obtained for other compounds (not shown). The harmonic and intermodulation peaks are clearly visible and are much larger than the background noise. The two large peaks, with amplitude of about 200 µA, are the response to the 40 and 100 mHz (2 and 5 Hz) excitation frequencies. It is important to note that between the peaks there is nearly no current response (< 100 nA). The experimental EFM data were treated using two different models: complete diffusion control of the cathodic reaction and the "activation" model. For the latter, a set of three non-linear equations had been solved, assuming that the corrosion potential does not change due to the polarization of the working electrode [22]. The larger peaks were used to calculate the corrosion current density (i_{corr}), the Tafel slopes (β_c and β_a) and the

causality factors (CF-2 and CF-3). These electrochemical parameters were listed in Table 3. The data presented in Table 3 obviously show that, the addition of any one of tested compounds at a given concentration to the acidic solution decreases the corrosion current density, indicating that these compounds inhibit the corrosion of copper in 2 M HNO_3 through adsorption. The causality factors obtained under different experimental conditions are approximately equal to the theoretical values (2 and 3) indicating that the measured data are verified and of good quality. The inhibition efficiencies $\%IE_{EFM}$ increase by increasing the inhibitor concentrations and calculated from equation (1):

$$\% \ IE_{EFM} = [1-(i_{corr}/ \ i^{o}_{corr} \ )] \times 100 \tag{1}$$

where i^{o}_{corr} and i_{corr} are corrosion current densities in the absence and presence of inhibitor, respectively.
The inhibition sufficiency obtained from this method is in the order:

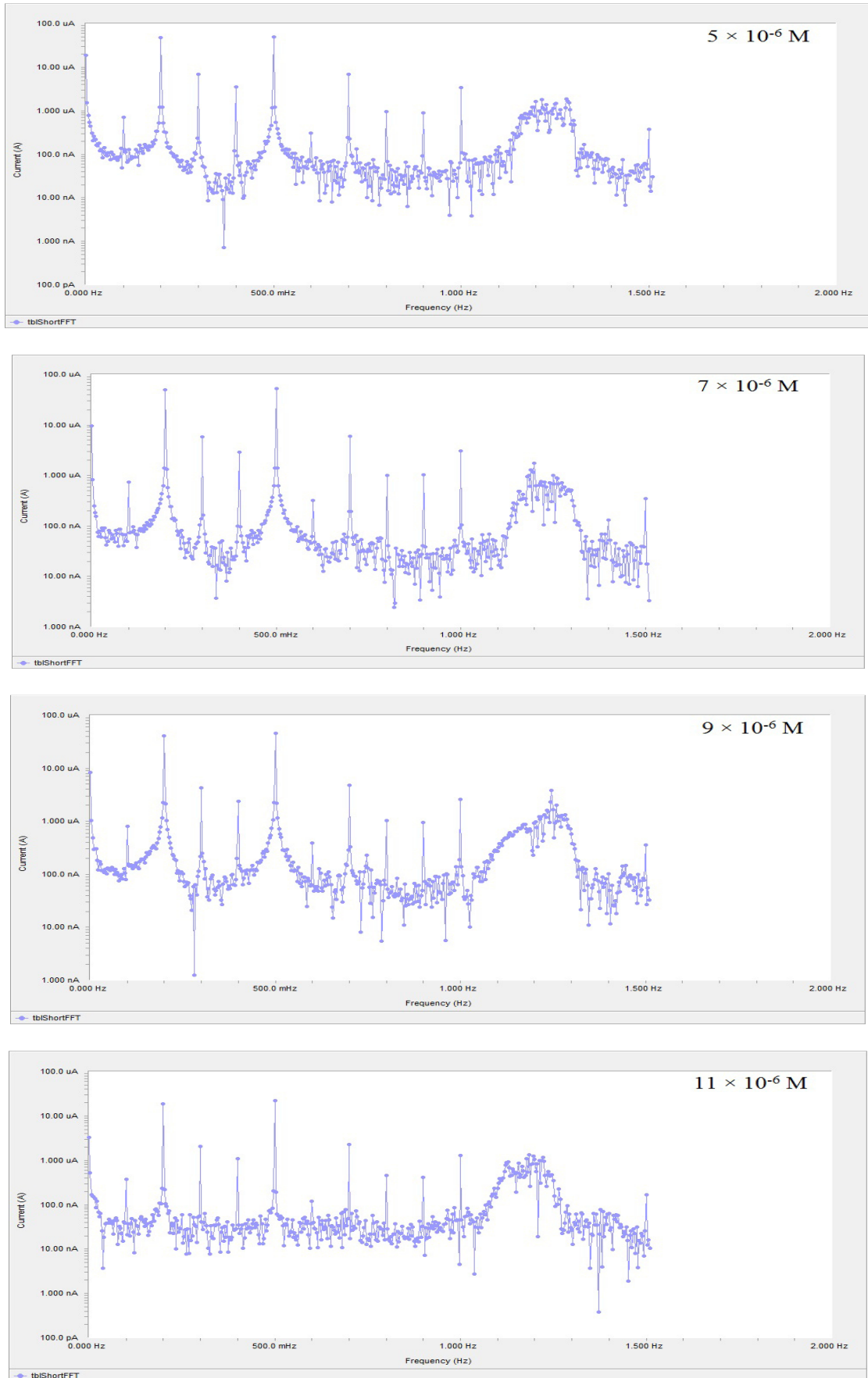compound (I) > compound (II) > compound (III).
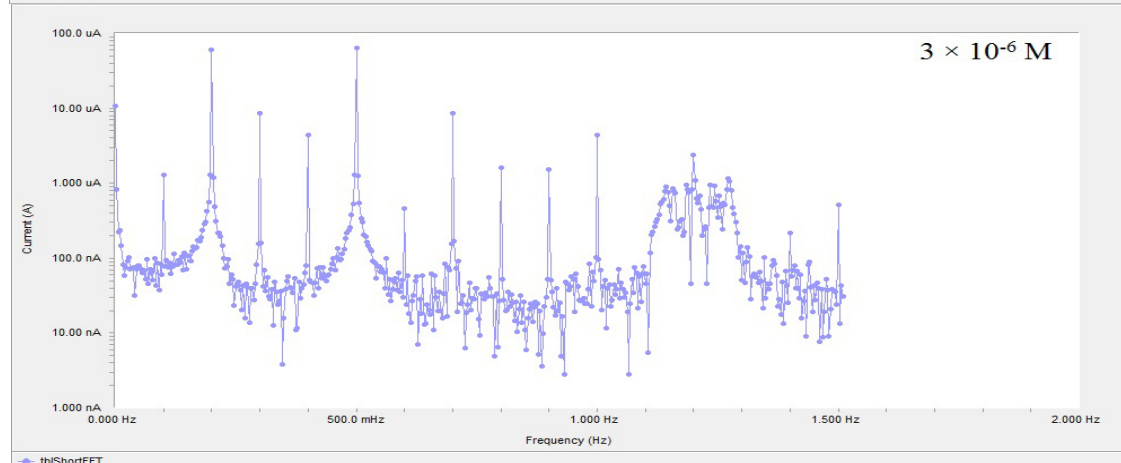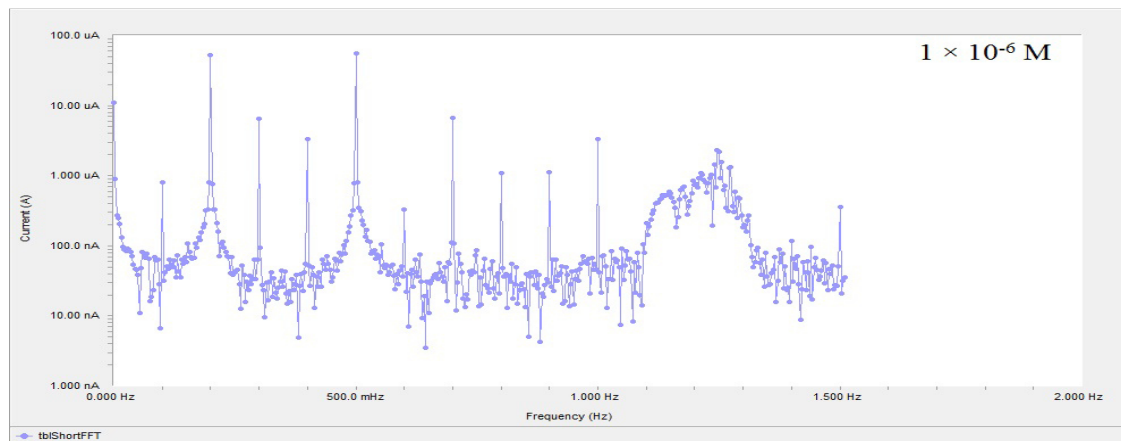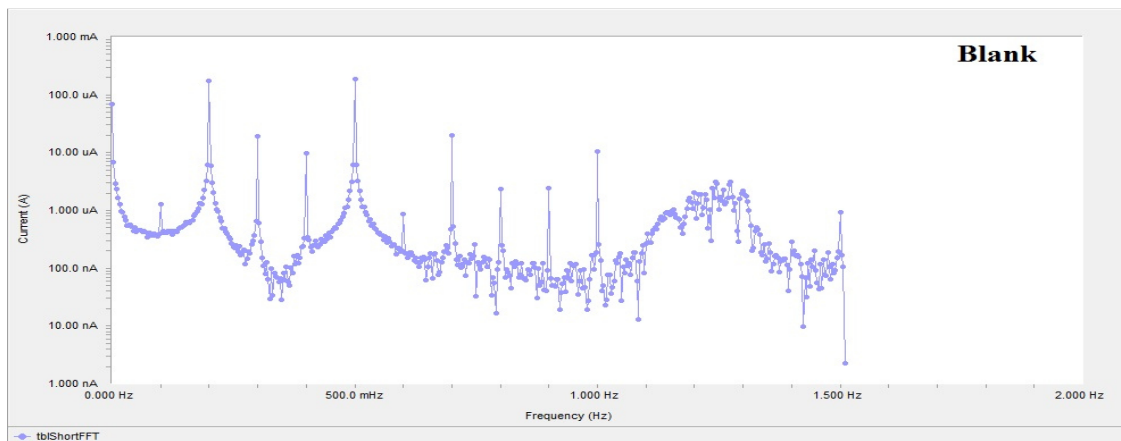
Figure 1: EFM spectra for copper in 2 M HNO$_3$ in the abscence and presence of different concentrations of compound (I).

Table 3: Electrochemical kinetic parameters obtained by EFM technique for copper in 2 M HNO$_3$ without and with various concentrations of compounds (I-III) at 30 ^{o}C.

Comp.	Conc. (M)	i_{corr} ($\mu A\ cm^{-2}$)	$\beta_{a} \times 10^{-3}$ (mV dec^{-1})	$\beta_{c} \times 10^{-3}$ (mV dec^{-1})	CF-2	CF-3	θ	%IE
Blank	-----	388.6	95.1	260.6	1.95	2.3	-----	-----
I	1×10^{-6}	88.3	75.9	175.1	1.98	2.7	0.773	77.3
	3×10^{-6}	76.5	59.9	121.8	1.94	3.5	0.803	80.3
	5×10^{-6}	73.2	68.6	166.9	1.97	3.0	0.811	81.1
	7×10^{-6}	69.2	67.2	127.5	1.94	3.4	0.822	82.2
	9×10^{-6}	58.87	68.6	122.4	1.83	2.5	0.849	84.9
	11×10^{-6}	23.5	59.8	98.8	1.85	3.0	0.940	94.0
II	1×10^{-6}	193.1	69.7	155.7	1.95	2.8	0.503	50.3
	3×10^{-6}	174.1	84.9	191.5	1.93	2.7	0.552	55.2
	5×10^{-6}	165.7	74.8	167.7	1.95	3.0	0.574	57.4
	7×10^{-6}	140.5	71.24	207.3	1.95	2.8	0.638	63.8
	9×10^{-6}	128.7	77.3	176.9	1.91	2.7	0.669	66.9
	11×10^{-6}	109.4	77.6	173.5	1.99	2.8	0.718	71.8
III	1×10^{-6}	372.6	101.3	397.9	1.91	2.3	0.041	4.1
	3×10^{-6}	296.1	82.9	169.3	1.92	2.6	0.238	23.8
	5×10^{-6}	249.1	63.0	128.3	1.96	3.5	0.359	35.9
	7×10^{-6}	233.3	70.1	145.3	1.97	3.1	0.400	40.0
	9×10^{-6}	230.6	79.7	190.6	1.95	2.6	0.407	40.7
	11×10^{-6}	199.4	83.3	213.3	1.94	2.7	0.487	48.7

3.2. Electrochemical impedance spectroscopy (EIS)

EIS is well-established and powerful technique in the study of corrosion. Surface properties, electrode kinetics and mechanistic information can be obtained from impedance diagrams [23-25]. Figure 2 shows the Nyquist (a) and Bode (b) plots obtained at open-circuit potential both in the absence and presence of increasing concentrations of investigated compounds at 30 °C.

The increase in the size of the capacitive loop with the addition of organic derivatives shows that a barrier gradually forms on the copper surface. The increase in the capacitive loop size (Figure 2a) enhances, at a fixed inhibitor concentration, following the order: compound (I) > compound (II) > compound (III), confirming the highest inhibitive influence of compound (I). Bode plots (Figure 2b), shows that the total impedance increase with increasing inhibitor concentration (log Z *vs.* log f). But (log f *vs.* phase), also Bode plot shows the continuous increase in the phase angle shift, obviously correlating with the increase of inhibitor adsorbed on copper surface. The Nyquist plots do not yield perfect semicircles as expected from the theory of EIS. The deviation from ideal semicircle was generally attributed to the frequency dispersion [26,27] as well as to the inhomogenities of the surface.

EIS spectra of the organic additives were analyzed using the equivalent circuit, Figure 3, which represents a single charge transfer reaction and fits well with our experimental results. The constant phase element, CPE, is introduced in the circuit instead of a pure double layer capacitor to give a more accurate fit [28].The double layer capacitance, C_{dl}, for a circuit including a CPE parameter (Y_o and n) were calculated from equation (2) [29]:

$$C_{dl} = Y_o\ \omega^{n-1} / \sin [n\ (\pi/2)] \tag{2}$$

where Y_o is the magnitude of the CPE, $\omega = 2\pi f_{max}$, f_{max} is the frequency at which the imaginary component of the impedance is maximal and the factor n is an adjustable parameter that usually lies between 0.50 and 1.0.

After analyzing the shape of the Nyquist plots, it is concluded that the curves approximated by a single capacitive semicircles, showing that the corrosion process was mainly charged-transfer controlled [30]. The general shape of the curves is very similar for all samples (in presence or absence of inhibitors at different immersion times) indicating that no change in the corrosion mechanism [27]. From the impedance data as listed in Table 4, we conclude that the value of R_{ct} increase with increasing the concentration of the inhibitors and this indicates an increase in %IE, which in concord with the EFM results obtained.
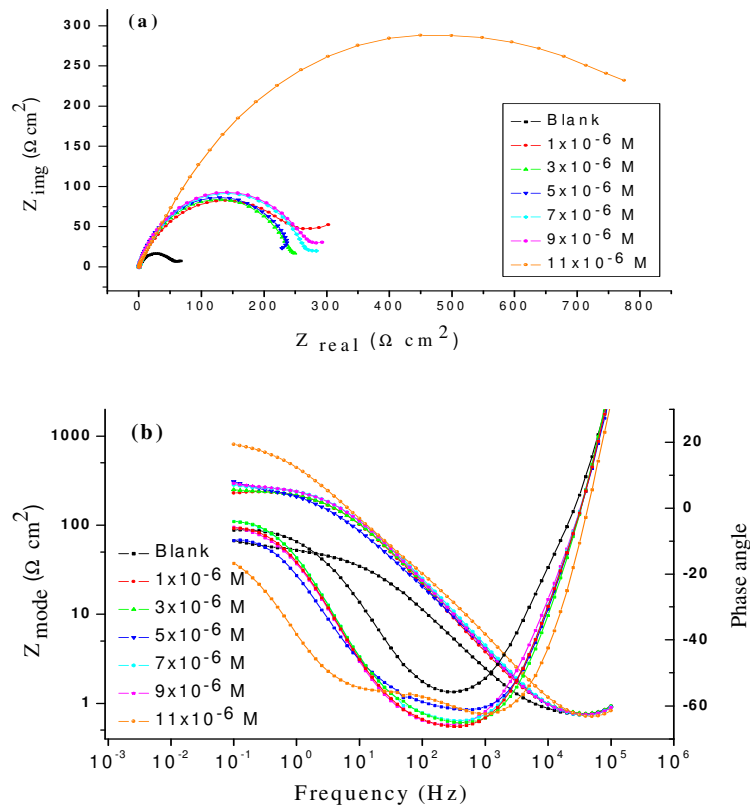
J. Mater. Environ. Sci. 6 (8) (2015) 2260-2276
ISSN : 2028-2508
CODEN: JMESCN

El-Sonbati et al.

Figure 2: EIS Nyquist plots (a) and Bode plots (b) for copper in 2 M HNO_3 in the absence and presence of different concentrations of compound (I).

Table 4: Electrochemical kinetic parameters obtained from EIS technique for copper in 2 M HNO_3 in the absence and presence of different concentrations of compounds (I-III).

Comp.	Conc. (M)	$R_{S \times 10^{-3}}$ $(\Omega\ cm^2)$	$Y_{o \times 10^{-6}}$	$n_{\times 10^{-3}}$	R_{ct} $(\Omega\ cm^2)$	$C_{dl \times 10^{-4}}$ $(\mu F cm^{-2})$	θ	%IE
Blank	------	710.4	656.5	758.3	55.81	2.483	------	------
I	1×10^{-6}	719.5	398.2	807.5	238.4	0.902	0.766	76.6
	3×10^{-6}	703.1	256.4	799.7	239.6	0.855	0.767	76.7
	5×10^{-6}	646.8	258.9	754.0	262.0	0.836	0.787	78.7
	7×10^{-6}	668.9	233.8	801.9	263.3	0.809	0.788	78.8
	9×10^{-6}	689.6	234.6	809.6	267.1	0.775	0.791	79.1
	11×10^{-6}	564.6	373.3	722.8	870.0	0.571	0.936	93.6
II	1×10^{-6}	672.6	465.9	757.5	116.4	1.332	0.521	52.1
	3×10^{-6}	750.2	365.1	779.8	117.9	1.277	0.527	52.7
	5×10^{-6}	569.6	353.0	782.9	148.8	1.191	0.625	62.5
	7×10^{-6}	655.2	358.7	770.3	170.4	1.101	0.672	67.2
	9×10^{-6}	646.2	257.9	817.1	212.2	1.012	0.737	73.7
	11×10^{-6}	712.4	232.8	812.2	233.4	0.968	0.761	76.1
III	1×10^{-6}	652.9	637.4	745.9	60.92	2.276	0.084	8.4
	3×10^{-6}	725.2	652.9	748.5	65.99	2.243	0.154	15.4
	5×10^{-6}	585.6	560.3	758.0	78.58	1.948	0.290	29.0
	7×10^{-6}	651.0	425.3	780.6	85.76	1.601	0.349	34.9
	9×10^{-6}	625.9	418.5	784.9	89.25	1.592	0.375	37.5
	11×10^{-6}	604.9	377.8	778.5	110.6	1.469	0.495	49.5

In fact the presence of inhibitors enhances the value of R_{ct} in acidic solution. Values of double layer capacitance are also brought down to the maximum extent in the presence of inhibitor and the decrease in the values of CPE follows the order similar to that obtained for i_{corr} in this study. The decrease in CPE/C_{dl} results from a decrease in local dielectric constant and/or an increase in the thickness of the double layer, suggesting that organic derivatives inhibit the iron corrosion by adsorption at metal/acid [31]. The inhibition efficiency was calculated from the charge transfer resistance data from equation (3) [27]:

$$ \% \ IE_{EIS} = [1- (R^{\circ}_{ct}/R_{ct})] \times 100 \tag{3} $$

where R^{o}_{ct} and R_{ct} are the charge-transfer resistance values without and with inhibitor, respectively.
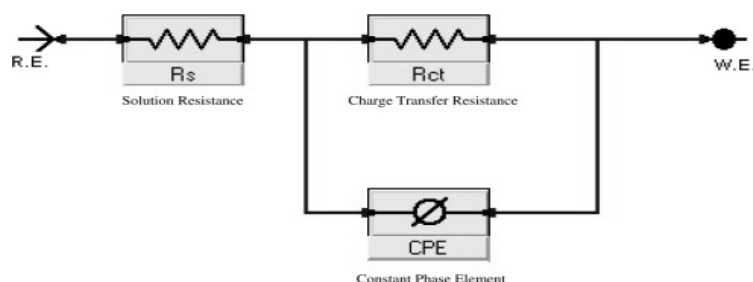

Figure 3: Equivalent circuit model used to fit experimental EIS

3.3. Potentiodynamic polarization measurements

Theoretically, copper can hardly be corroded in the deoxygenated acid solutions, as copper cannot displace hydrogen from acid solutions according to the theories of chemical thermodynamics [32,33]. However, this situation will change in nitric acid. Dissolved oxygen may be reduced on copper surface and this will allow corrosion to occur. It is a good approximation to ignore the hydrogen evolution reaction and only consider oxygen reduction in the nitric acid solutions at potentials near the corrosion potentials [34].

Polarization measurements were carried out in order to gain knowledge concerning the kinetics of the cathodic and anodic reactions. Figure 4, shows the polarization behavior of copper electrode in 2 M HNO_3 in the absence and presence of various concentrations of compound (I). Similar curves were obtained for other inhibitors (not shown). Figure 4 shows that both the anodic and cathodic reactions are affected by the addition of investigated organic derivatives and the inhibition efficiency increases as the inhibitor concentration increases, but the cathodic reaction is more inhibited, meaning that the addition of organic derivatives reduces the anodic dissolution of copper and also retards the cathodic reactions. Therefore, investigated organic derivatives are considered as mixed type inhibitors.

The values of electrochemical parameters such as corrosion current densities (i_{corr}), corrosion potential (E_{corr}), the cathodic Tafel slope (β_c), anodic Tafel slope (β_a) and inhibition efficiency (%IE) were calculated from the curves of Figure 4 and are listed in Table (5). The results in Table (5) revealed that the corrosion current density decreases obviously after the addition of inhibitors in 2 M HNO_3 and %IE increase with increasing the inhibitor concentration. In the presence of inhibitors E_{corr} was enhanced with no definite trend, indicating that these compounds act as mixed–type inhibitors in 2 M HNO_3. The inhibition efficiency was calculated using equation (4):

$$ \% IE_p = [(i^{o}_{corr} - i_{corr}) / i^{o}_{corr}] \times 100 \tag{4} $$

where i^{o}_{corr} and i_{corr} are the uninhibited and inhibited corrosion current densities, respectively.

Also it is obvious from Table 5, that the slopes of the anodic (β_a) and cathodic (β_c) Tafel lines remain almost unchanged upon addition of organic derivatives, giving rise to a nearly parallel set of anodic lines, and almost parallel cathodic plots results too. Thus the adsorbed inhibitors act by simple blocking of the active sites for both anodic and cathodic processes. In other words, the adsorbed inhibitors decrease the surface area for corrosion without affecting the corrosion mechanism of copper in 2 M HNO_3 solution, and only cause inactivation of a part of the surface with respect to the corrosive medium [35].

The inhibition efficiency of these compounds follows the sequence: compound (I) > compound (II) > compound (III). This sequence may attribute to free electron pair in oxygen atom, π electrons on aromatic nuclei and the substituent in the molecular structure of the inhibitor and again reflects, as confirmed from EFM and EIS measurements, the increased ability of compound (I) to inhibit nitric acid corrosion of copper as compared to compound (III). This is clearly seen from the highest efficiency recorded for compound (I).
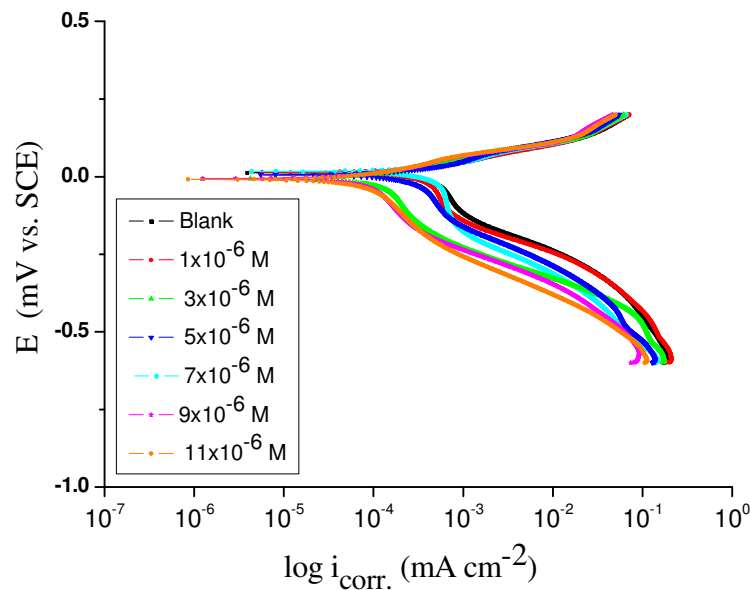
Figure 4: Potentiodynamic polarization curves for the corrosion of copper in 2 M HNO$_3$ in the absence and presence of various concentrations of compound (I) at 30 °C

Table 5: The effect of concentration of compounds (I-III) on the free corrosion potential (E$_{corr}$), corrosion current density (i$_{corr}$), Tafel slopes (β$_a$ & β$_c$), inhibition efficiency (%IE) and degree of surface coverage for the corrosion of copper in 2 M HNO$_3$ at 30 °C.

Comp.	Conc. (M)	- E$_{corr \times 10}^{-3}$ (mV vs. SCE)	i$_{corr \times 10}^{-4}$ (μA cm^{-2})	β$_{a \times 10}^{-3}$ (mV dec^{-1})	β$_{c \times 10}^{-3}$ (mV dec^{-1})	θ	%IE
Blank	-----	127	9.60	21.4	29.4	-----	-----
I	1×10^{-6}	940	1.28	82.2	68	0.867	86.7
	3×10^{-6}	586	1.26	69.4	79	0.869	86.9
	5×10^{-6}	555	1.18	32.3	59	0.877	87.7
	7×10^{-6}	167	1.12	22.2	34	0.883	88.3
	9×10^{-6}	695	1.07	57.8	152	0.889	88.9
	11×10^{-6}	137	1.06	24.2	39	0.890	89.0
II	1×10^{-6}	769	2.05	65.5	195	0.786	78.6
	3×10^{-6}	703	2.00	83.4	455	0.792	79.2
	5×10^{-6}	588	1.80	41.8	86	0.813	81.3
	7×10^{-6}	119	1.51	28.7	43	0.843	84.3
	9×10^{-6}	934	1.47	48.5	137	0.847	84.7
	11×10^{-6}	128	1.37	27.5	42	0.860	85.7
III	1×10^{-6}	282	8.43	77.8	203	0.122	12.2
	3×10^{-6}	497	5.56	90.9	158	0.421	42.1
	5×10^{-6}	105	5.33	74.3	492	0.445	44.5
	7×10^{-6}	161	3.87	53.3	289	0.597	59.7
	9×10^{-6}	197	2.36	76.5	88.3	0.754	75.4
	11×10^{-6}	905	2.29	50.7	171	0.760	76.0

3.4. Weight loss measurements

Figure 5 represents the weight loss-time curves for copper in 2 M HNO$_3$ in the absence and presence of different concentrations of compound (HL$_1$). Similar curves were obtained for other inhibitors (not shown). Table 6 collects the values of inhibition efficiency obtained from weight loss measurements in 2 M HNO$_3$ at

30 °C. The results of this Table show that the presence of inhibitors reduces the corrosion rate of copper in 2 M HNO_3 and hence, increase the inhibition efficiency. The inhibition achieved by these compounds decreases in the following order:

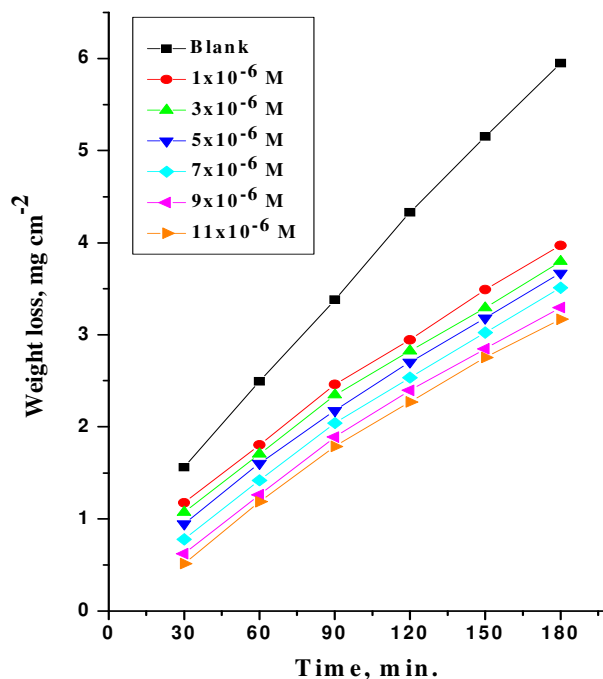compound (I) > compound (II) > compound (III).

Figure 5: Weight-loss time curves for the dissolution of copper in the absence and presence of different concentrations of compound (I) at 30 °C.

Table 6: Variation of inhibition efficiency (%IE) of investigated compounds (I-III) with their molar concentrations at 30 °C from weight loss measurements at 120 min immersion in 2 M HNO_3

Conc. (M)	Inhibition efficiency (%IE)		
	I	II	III
1×10^{-6}	31.99	30.26	29.33
3×10^{-6}	34.79	33.72	31.72
5×10^{-6}	37.58	37.45	35.65
7×10^{-6}	41.44	40.51	38.94
9×10^{-6}	44.64	43.17	42.81
11×10^{-6}	47.56	46.90	45.25

The inhibition efficiencies, calculated from EFM, EIS and polarization show the same trend as those obtained from weight loss measurements. The difference of inhibition efficiency from the four methods may be attributed to the different surface status of the electrode in the four measurements. EIS were performed at the rest potential, while in polarization measurements the electrode potential was polarized to high over potential, non-uniform current distributions, resulted from cell geometry, solution conductivity, counter and reference electrode placement, etc., will lead to the difference between the electrode area actually undergoing polarization and the total area [36].

3.5. Adsorption isotherm

Basic information on the interaction between the inhibitor and the metal surface can be provided by the adsorption isotherm, and the type of the inhibitors on metal is influenced by (i) the nature and charge of the metal (ii) chemical structure of the inhibitor and (iii) the type of electrolyte.

The values of (θ) for different concentrations of the studied compounds at 30 ^oC have been used to explain the best isotherm to determine the adsorption process. The adsorption of the organic derivatives, on the surface of copper electrode may regarded as a substitution adsorption process between organic compounds in aqueous phase (org_{aq}) and the water molecules adsorbed on Cu surface (H_2O_{ads}) [37]:

$$Org_{(sol)} + x (H_2O)_{ads} \leftrightarrow Org_{(ads)} + x H_2O_{(sol)} \tag{5}$$

where x is the number of water molecules replaced by one organic molecule. Attempts were made to fit (θ) values to various isotherms, including Langmuir [38], Frumkin [39], Temkin and Freundlich isotherms [40]. In this study, The plot of log θ versus log C is shown in Figure 6, yielded straight line curve clearly proving that the adsorption of these inhibitors from 2 M HNO_3 solution on copper surface obeys Freundlich adsorption isotherm:

$$\log \theta = \log K_{ads} + n \log C \tag{6}$$

where K_{ads} is the adsorption equilibrium constant, n is the interaction parameter and C is the inhibitor concentration.
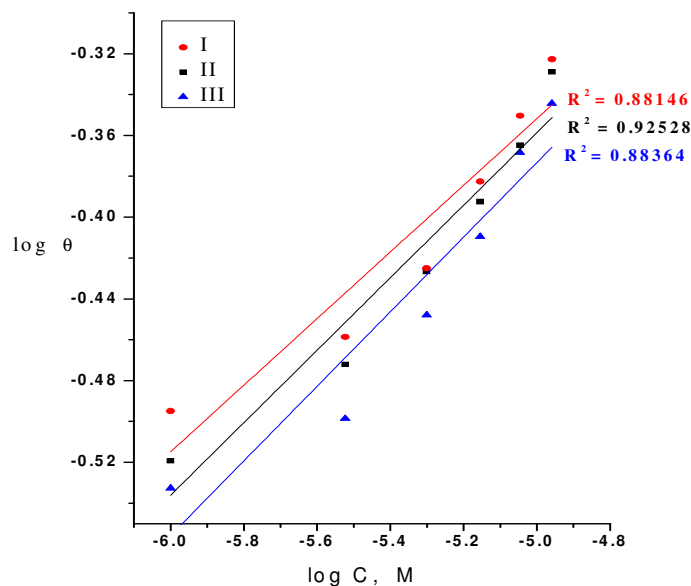

Figure 6: Curve fitting of corrosion data for copper in 2 M HNO_3 in presence of different concentrations of compounds (I-III) additives to the Freundlich isotherm at 30 °C.

Equilibrium constant (K_{ads}) of adsorption process determined using equation (6) could be further used to determine free energy of adsorption (ΔG^o_{ads}) as follows:

$$\Delta G^o_{ads} = -RT \ln (55.5 K_{ads}) \tag{7}$$

where 55.5 is the concentration of water in the solution in M/L.

The calculated values of K_{ads}, the interaction parameter (n) and ΔG°_{ads} are given in Table 7. From these results it may be generalized that the more efficient inhibitor has more negative ΔG°_{ads} value so that from the Tabulated values of ΔG°_{ads} the order of inhibition efficiency is as follows: compound (I) > compound (II) > compound (III).

The negative value of $\Delta G°_{ads}$ for organic compounds ensures that spontaneity of the adsorption process and the stability of adsorbed layer on the copper surface. The values of K_{ads} were found to run parallel to the %IE [K_{ads} (I) > K_{ads} (II) > K_{ads} (III)]. This result reflects the increasing capability, due to structural formation, on the metal surface [27].

Table 7: Adsorption equilibrium constant (K_{ads}), the interaction parameter (n) and free energy of adsorption ($\Delta G°_{ads}$) of inhibitors with their molar concentrations at 30 $°C$ from weight loss measurements at 120 min immersion in 2 M HNO_3

Compound	K_{ads}	n	$-\Delta G°_{ads}$ (kJ mol^{-1})
I	0.296	0.038	7.06
II	0.283	0.037	6.94
III	0.269	0.035	6.81

An inspection of the results in Table 7 reveals that the values of K_{ads} and $-\Delta G°_{ads}$ of compounds (I-III) are influenced by the inductive or mesmeric effect of the substituents. Compound (I) has a lower acidic character (higher K_{ads} values) than compound (II). This is quite reasonable because the presence of p-OCH_3 group (i.e. an electron-donating effect). The presence of p-NO_2 group (i.e. an electron-withdrawing effect) will lead to the opposite effect (has a lower value of K_{ads}). The results are also in accordance with values of Hammett's substituent coefficients (σ^R). Straight lines are obtained on plotting the relationship between σ^R *vs*. K_{ads} and $-\Delta G°_{ads}$ values a shown in Fig. 7.

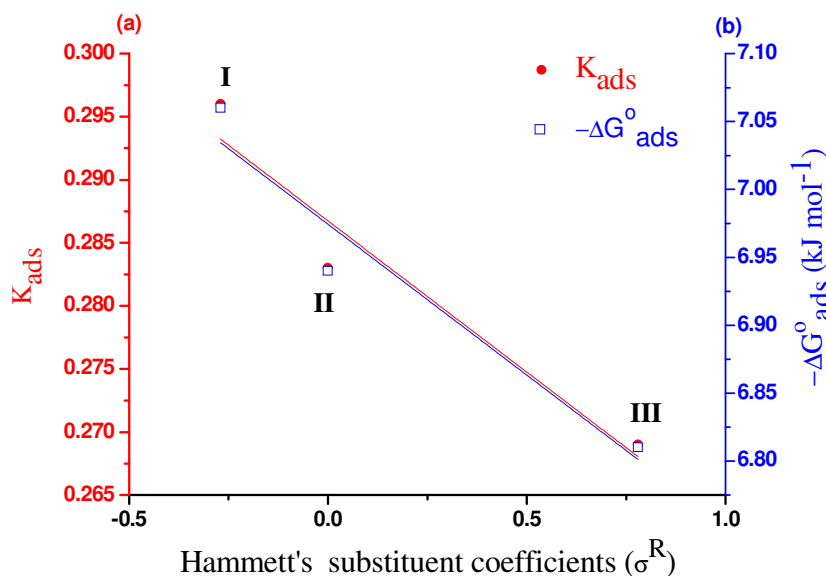**Figure 7:** The relation between Hammett's substituent coefficients (σ^R) *vs*. a) K_{ads} and b) $-\Delta G°_{ads}$ of compounds (I-III).

3.6. Effect of temperature
The effect of temperature on the inhibited acid-metal reaction is highly complex, because many changes occur on the metal surface, such as rapid etching and desorption of the inhibitor and the inhibitor itself, in some cases, may undergo decomposition and/or rearrangement.

Generally the corrosion rate increases with the rise of temperature. It was found that the inhibition efficiency decreases with increasing temperature and increase with increasing the concentration of the inhibitor. The activation energy (E^*_a) of the corrosion process was calculated using Arrhenius equation (8) [41]:

$$k = A \exp(-E^*_a / RT) \tag{8}$$

where k is the corrosion rate, A is Arrhenius constant, R is the gas constant and T is the absolute temperature.

The values of activation energies E_a^* can be obtained from the slope of the straight lines of plotting log k *vs.* 1/T in the presence and absence of investigated compounds at various temperatures as given in Figure 8 and Table 8, it is noted that the values of activation energy increase in the presence of inhibitors and with increase of the concentration of the inhibitors. This is due to the presence of a film of inhibitors on copper surface. The activation energy for the corrosion of copper in 2 M HNO$_3$ was found to be 41.15 kJ mol^{-1} which is in good agreement with the work carried out by Fouda et al. [42] and others [43]. An alternative formulation of the Arrhenius equation is the transition state equation (9) [44]:

$$k = RT/Nh \exp (\Delta S^*/R) \exp (-\Delta H^*/ RT) \tag{9}$$

where h is Planck's constant, N is Avogadro's number, ΔS^* is the entropy of activation and ΔH^* is the enthalpy of activation. Figure 9 shows a plot of log (k/T) *vs.* (1/T). Straight lines are obtained with a slope of ($\Delta H^*/2.303$ R) and an intercept of (log R/Nh + $\Delta S^*/2.303$ R) from which the values of ΔH^* and ΔS^* are calculated and also listed in Table 8. From inspection of Table 8, it is clear that the positive values of ΔH^* reflect that the process of adsorption of the inhibitors on the copper surface is an endothermic process; it is attributable unequivocally to chemisorption. Typically, the enthalpy of a chemisorption process approaches 100 kJ mol^{-1} [45]. More interesting behavior was observed in Table 8, that positive values of ΔS^* are accompanied with endothermic adsorption process. This is agrees with what expected, when the adsorption is an endothermic process, it must be accompanied by an increase in the entropy energy change and vies versa [37].

It is seen that investigated derivatives have inhibiting properties at all the studied temperatures and the values of %IE decrease with temperature increase. This shows that the inhibitor has experienced a significant decrease in its protective properties with increase in temperature. This decrease in the protective properties of the inhibitor with increase in temperature may be connected with two effects; a certain drawing of the adsorption-desorption equilibrium towards desorption (meaning that the strength of adsorption process decreases at higher temperatures) and roughening of the metal surface which results from enhanced corrosion. These results suggest that physical adsorption may be the type of adsorption of the inhibitor on the copper surface.
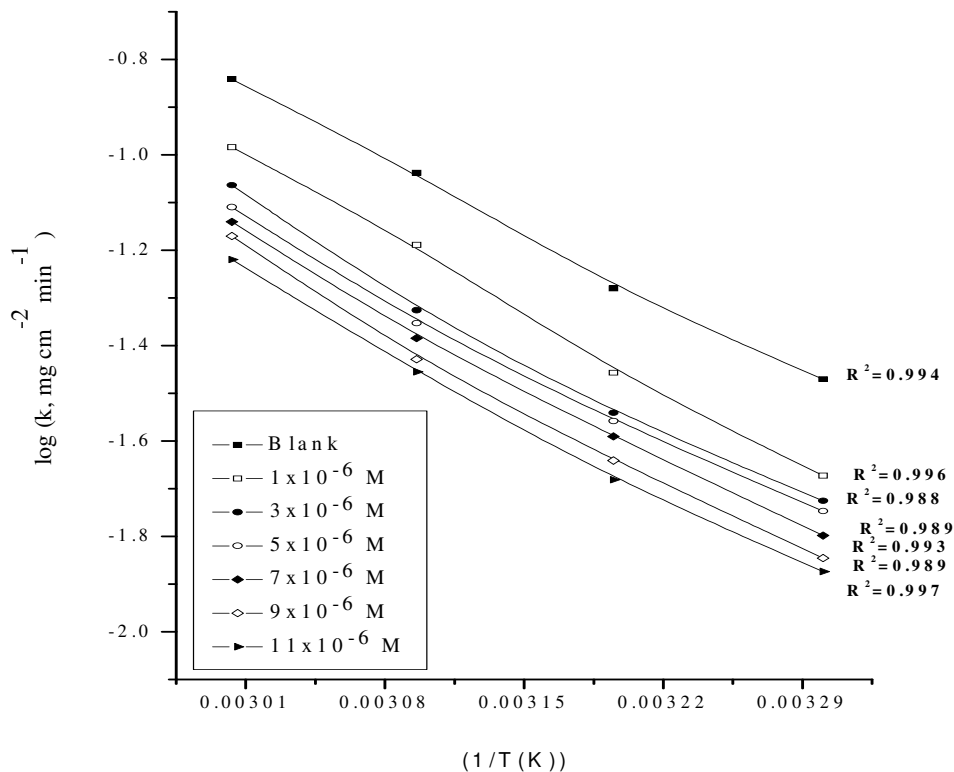

Figure 8: Arrhenius (log k *vs.* 1/T) for corrosion of copper in 2 M HNO$_3$ in the absence and presence of different concentrations of compound (I).
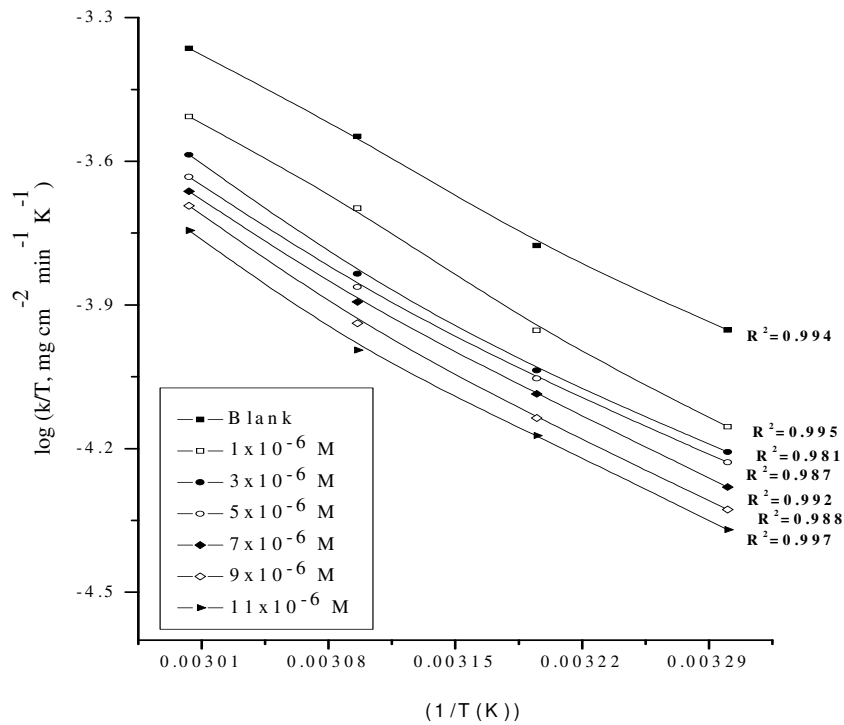
J. Mater. Environ. Sci. 6 (8) (2015) 2260-2276
ISSN : 2028-2508
CODEN: JMESCN

El-Sonbati et al.

Figure 9: Plots of (log k/T) *vs.* 1/T for corrosion of copper in 2 M HNO₃ in the absence and presence of different concentrations of compound (I).

Table 8: Thermodynamic activation parameters for the dissolution of copper in 2 M HNO₃ in the absence and presence of different concentrations of compounds (I-III).

Comp.	Conc. (M)	E_a^* (kJ mol^{-1})	ΔH^* (kJ mol^{-1})	$-\Delta S^*$ (J mol^{-1} K^{-1})
Blank	-----	41.15	38.51	146.59
I	1×10^{-6}	42.26	39.07	146.86
	3×10^{-6}	42.37	39.12	147.74
	5×10^{-6}	43.05	39.41	148.97
	7×10^{-6}	43.10	40.07	148.99
	9×10^{-6}	43.20	40.16	149.11
	11×10^{-6}	42.24	40.60	150.27
II	1×10^{-6}	39.20	36.56	157.13
	3×10^{-6}	39.22	36.58	157.44
	5×10^{-6}	40.15	37.51	158.04
	7×10^{-6}	40.42	37.78	158.70
	9×10^{-6}	41.06	38.42	159.37
	11×10^{-6}	41.08	38.44	159.74
III	1×10^{-6}	39.06	36.12	159.44
	3×10^{-6}	38.69	36.55	159.54
	5×10^{-6}	38.77	35.63	159.63
	7×10^{-6}	38.82	36.69	159.95
	9×10^{-6}	38.88	36.74	160.06
	11×10^{-6}	38.92	36.98	160.10

3.7. Quantum chemical calculations

Figure 10 represents the molecular orbital plots and Mulliken charges of investigated compounds. Theoretical calculations were performed for only the neutral forms, in order to give further insight into the experimental results. Values of quantum chemical indices such as energies of lowest unoccupied molecular orbitals (LUMO) and energy of highest occupied molecular orbitals (HOMO) (E_{HOMO} and E_{LUMO}) and energy gap (ΔE) are calculated as given in Table 9. It has been reported that the higher or less negative E_{HOMO} is associated of inhibitor, the greater the trend of offering electrons to unoccupied d orbital of the metal, and the higher the corrosion inhibition efficiency, in addition, the lower E_{LUMO}, the easier the acceptance of electrons from metal surface [46].
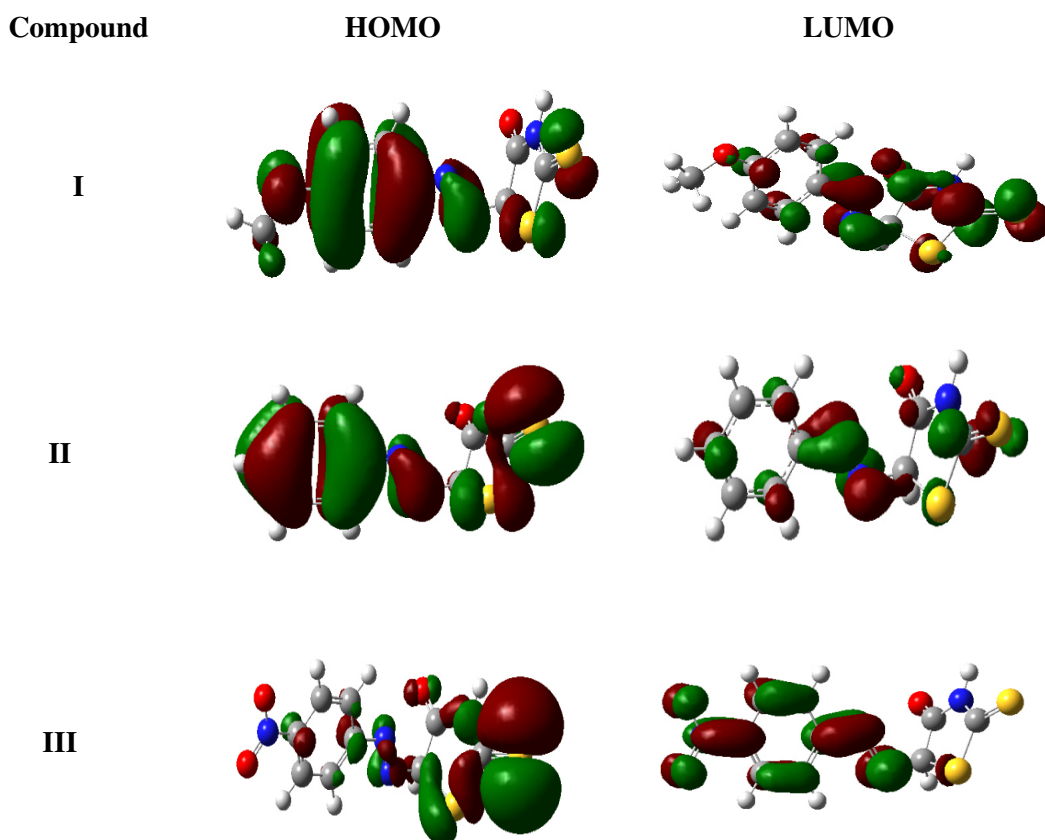
Compound	HOMO	LUMO

Figure 10: The highest occupied molecular orbital (HOMO) and the lowest unoccupied molecular orbital (LUMO) of compounds (I-III).

Table 9: The calculated quantum chemical properties for compounds (I-III).

Comp.	E_{HOMO} (a.u.)	E_{LUMO} (a.u.)	ΔE (a.u.)	μ (D)	T.E (a.u.)	χ (a.u.)	η (a.u.)	σ (a.u.)$^{-1}$	Pi (a.u.)	S (a.u.)$^{-1}$	ω (a.u.)	ΔN_{max} (a.u.)
I	-0.327	-0.048	0.279	5.358	-1491.580	0.139	0.188	5.333	-0.139	2.667	0.052	0.744
II	-0.348	-0.044	0.304	3.950	-1377.752	0.152	0.196	5.102	-0.152	2.551	0.059	0.776
III	-0.367	-0.004	0.363	3.712	-1581.099	0.186	0.182	5.509	-0.186	2.755	0.095	1.022

From Table 9, it is clear that ΔE obtained by the three methods in case of compound (I) is lower than other two compounds, which enhance the assumption that compound (I) molecule will absorb more strongly on copper surface than other two compounds, due to facilitating of electron transfer between molecular orbital HOMO and LUMO which takes place during its adsorption on the metal surface and thereafter presents the maximum of inhibition efficiency. Also it can be seen that E_{HOMO} increases from compound (I) to compound (III) facilitates the adsorption and the inhibition by supporting the transport process through the adsorbed layer. Reportedly, excellent corrosion inhibitors are usually those organic compounds who are not only offer electrons to

unoccupied orbital of the metal, but also accept free electrons from the metal [47]. It can be seen that all calculated quantum chemical parameters validate these experimental results.

3.8. Inhibition mechanism
Inhibition of the corrosion of copper in 2 M HNO_3 solution by investigated compounds is determined by weight loss, potentiodynamic polarization measurements, electrochemical impedance spectroscopy (EIS) and electrochemical frequency modulation method (EFM), it was found that the inhibition efficiency depends on concentration, nature of metal, the mode of adsorption of the inhibitors and surface conditions.
The observed corrosion data in presence of these inhibitors, namely:
        i) the decrease of corrosion rate and corrosion current with increase in concentration of the inhibitor. ii) the linear variation of weight loss with time. iii) the shift in Tafel lines to higher potential regions. iv) the decrease in corrosion inhibition with increasing temperature indicates that desorption of the adsorbed inhibitor molecules takes place and v) the inhibition efficiency was shown to depend on the number of adsorption active centers in the molecule and their charge density.
The corrosion inhibition is due to adsorption of the inhibitors at the electrode / solution interface, the extent of adsorption of an inhibitor depends on the nature of the metal, the mode of adsorption of the inhibitor and the surface conditions. Adsorption on copper surface is assumed to take place mainly through the active centers attached to the inhibitor and would depend on their charge density. Transfer of lone pairs of electrons on the nitrogen atoms to the copper surface to form a coordinate type of linkage is favored by the presence of a vacant orbital in copper atom of low energy. Polar character of substituents in the changing part of the inhibitor molecule seems to have a prominent effect on the electron charge density of the molecule.
It was concluded that the mode of adsorption depends on the affinity of the metal towards the π-electron clouds of the ring system. Metals such as Cu, which have a greater affinity towards aromatic moieties, were found to adsorb benzene rings in a flat orientation. The order of decreasing the percentage inhibition efficiency of the investigated inhibitors in the corrosive solution was as follow:
compound (I) > compound (II) > compound (III).
    Compound (I) exhibits excellent inhibition power due to: (i) the presence of *p*-OCH_3 group which is an electron donating group with negative Hammett constant (σ = -0.27), Also this group will increase the electron charge density on the molecule, and (ii) its larger molecular size that may facilitate better surface coverage.
    Compound (II) comes after compound (I) in inhibition efficiency. This is due to it has lesser molecular size and has no substituent in *p*-position (H-atom with σ =0.0) which contributes no charge density to the molecule.
    Compound (III) comes after compound (II) in inhibition efficiency. This is due to presence of *p*-NO_2 which has positive Hammett constant (σ =+0.78).i.e. group which lower the electron density on the molecule and hence, lower inhibition efficiency.

Conclusions
1. The tested of azo rhodanine derivatives establish a very good inhibition for copper corrosion in HNO_3 solution.
2. Azo rhodanine derivatives inhibit copper corrosion by adsorption on its surface and act better than the passive oxide film.
3. The inhibition efficiency is in accordance to the order: compound (I) > compound (II) > compound (III).
4. The inhibition efficiencies of the tested compounds increase with increasing of their concentrations.
5. Double layer capacitances decrease with respect to blank solution when the inhibitor added. This fact may explained by adsorption of the inhibitor molecule on the copper surface.
6. The adsorption of these compounds on copper surface in 2 M HNO_3 solution follows Freundlich adsorption isotherm.
7. The values of inhibition efficiencies obtained from the different independent techniques showed the validity of the obtained results.

References
1. Jennings G.K., Laibinis P.E., Colloids and Surfaces A: *Physicochem & Eng. Asp.* 116 (1996) 105.
2. Sayed E.I., Sherif M., *Appl. Surf. Sci.* 252 (2006) 8615.
3. Szocs E., Vastag Gy., Shaban A., Kalman E., *Corros. Sci.* 47 (2005) 893.
4. Subramanian R., Lakshminarayanan V., *Corros. Sci.* 44 (2002) 535.
5. Ramesh S., Rajeswari S., *Corros. Sci.* 47 (2005) 151.
6. El-Naggar M.M., *Corros. Sci.* 42 (2002) 773.

7. Huynh N., Bottle S.E., Notoya T., Schweinsberg D.P., *Corros. Sci.* 44 (2002) 2583.
8. Stupnisek-Lisac E., Brnada A., Maance A.D., *Corros. Sci.* 42 (2000) 243.
9. Moretti G., Guidi F., *Corros. Sci.* 44 (2002) 1995.
10. Al Maofari A., Ezznaydy G., Idouli Y., Guédira F., Zaydoun S., Labjar N., El Hajjaji S., *J. Mater. Environ. Sci.* 5 (2014) 2081.
11. Galal A., Atta N.F., Hassan M.H., *Mater .Chem. Phys.* 89 (2005) 28.
12. El-Bindary A.A., El-Sonbati A.Z., Shoair A.F., Mohamed A.S., *J. Mater. Environ. Sci.* 6(6) (2015) 1723.
13. El-Sonbati A.Z., Diab M.A., El-Bindary A.A., Morgan Sh.M., *Spectrochim. Acta A* 127 (2014) 310.
14. Abou-Dobara M.I., El-Sonbati A.Z., Morgan Sh.M., *World J. Microbiol. Biotechnol.* 29 (2013) 119.
15. El-Sonbati A.Z., Diab M.A., El-Bindary A.A., Mohamed G.G., Morgan Sh.M., *Inorgan. Chim. Acta* 430 (2015) 96.
16. El-Sonbati A.Z., Diab M.A., El-Bindary A.A., Eldesoky A.M., Morgan Sh.M., *Spectrochim. Acta A* 135 (2015) 774.
17. Al-Sarawy A.A., Diab M.A., El-Desoky A.M., El-Bindary R.A., *Int. J. Sci. Eng. Res.* 4 (2013) 1510.
18. Abdel–Rehim S.S., Khaled K.F., Abd–Elshafi N.S., *Electrochim. Acta* 51 (2006) 3269.
19. Quraishi M.A., Sardar R., Jamal D., *Mater. Chem. Phys.* 71 (2001) 309.
20. El-Ghamaz N.A., El-Sonbati A.Z., Diab M.A., El-Bindary A.A., Awad M.K., Morgan Sh.M.*, Mater. Sci. Semicond. Process.* 19 (2014) 150.
21. Kus E., Mansfeld F., *Corros. Sci.* 48 (2006) 965.
22. Caigman G.A., Metcalf S.K., Holt E.M., *J.Chem. Cryst.* 30 (2000) 415.
23. Silverman D.C., Carrico J.E., *National Association of Corrosion Engineers* 44 (1988) 280.
24. Macdonald D.D., Mckubre M.C.H., "Impedance measurements in electrochemical systems," Modern Aspects of Electrochemistry, J.O'M. Bockris, B.E. Conway, R.E.White, Eds., Plenum Press, New York 14 (1982) pp. 61.
25. Fouda A.S., Shalabi K., Elmogazy H., *J. Mater. Environ. Sci.* 5 (2014) 1691.
26. El Achouri M., Kertit S., Gouttaya H.M., Nciri B., Bensouda Y., Perez L., Infante M.R., Elkacemi K., *Prog. Org. Coat.* 43 (2001) 267.
27. Fouda A.S., Eldesoky A.M., El-Sonbati A.Z., Salam S.F., *Int. J. Electrochem. Sci.* 9 (2014) 1867.
28. Macdonald J.R., Johanson W.B., in: J.R. Macdonald (Ed.), Theory in Impedance Spectroscopy, John Wiley& Sons, New York (1987) pp. 27.
29. Mertens S.F., Xhoffer C., Decooman B.C., Temmerman E., *Corrosion* 53 (1997) 381.
30. Trabanelli G., Montecelli C., Grassi V., Frignani A., *J. Cem. Concr. Res.* 35 (2005) 1804.
31. Lagrenee M., Mernari B., Bouanis M., Traisnel M., Bentiss F., *Corros. Sci.* 44 (2002) 573.
32. Ma H., Chen S., Niu L., Zhao S., Li S., Li D., *J. Appl. Electrochem.* 32 (2002) 65.
33. Quartarone G., Moretti G., Bellomi T., Capobianco G., Zingales A.*, Corrosion* 54 (1998) 606.
34. Smyrl W.H., in: J.O.M. Bockris, B.E. Conway, E. Yeager, R.E. White (Eds.), Comprehensive Treatise of Electrochemistry, Plenum Press, New York, (1981) p.116.
35. Schltze J.W., Wippermann K., *Electrochim. Acta* 32 (1987) 823.
36. Lebrini M., Lagrenée M., Traisnel M., Gengembre L., Vezin H., Bentiss F., *Appl. Surf. Sci.* 253 (2007) 9267.
37. Thomas J.M., Thomas W.J., Introduction to the Principles of Heterogeneous Catalysis, [5]th Ed., Academic Press, London (1981).
38. Langmuir I., *J. Am. Chem. Soc.,* 38 (1916) 2221.
39. Frumkin A.N., *Zeitschrift fur Physikalische Chemie* 116 (1925) 466.
40. El-Awady A., Abd El-Nabey B., Aziz G., *Electrochem. Soc.* 139 (1992) 2149.
41. Trabanelli G., in "Corrosion Mechanisms" (Ed. F. Mansfeld) Marcel Dekker, New York (1987) pp. 119.
42. Fouda A.S., Abd. El-Aal A., Kandil A.B., *J. Dasalination* 201 (2006) 216.
43. Fiala A., Chibani A., Darchen A., Boulkamh A., Djebbar K., *Appl. Surf. Sci.* 253 (2007) 9347.
44. Arab S.T., Noor E.M., *Corrosion* 49 (1993) 122.
45. Durnie W., Marco R.D., Jefferson A., Kinsella B., *J. Electrochem. Soc.* 146 (1999) 1751.
46. Samie F., Tidblad J., Kucera V., Leygraf C., *Atmospheric Environ.* 40 (2006) 3631.
47. Lukovits I., Pálfi K., Bakó I., Kálmán E., *Corrosion* 53 (1997) 915.

(2015) ; http://www.jmaterenvironsci.com